Title
Integrating Resonators to Catheters for MR-Guided Interventional Radiology

Author
Hu, Jeffrey

Publication Date
2015

Peer reviewed|Thesis/dissertation

Integrating Resonators to Catheters for MR-Guided Interventional Radiology

by

Jeffrey Hu

THESIS

Submitted in partial satisfaction of the requirements for the degree of

MASTER OF SCIENCE

in

Biomedical Imaging

in the

GRADUATE DIVISION

of the

UNIVERSITY OF CALIFORNIA, SAN FRANCISCO

Acknowledgement

I would like to thank Dr. Steven Hetts for the opportunity to work on the magnetic catheter project, along with Dr. David Saloner and Dr. Alastair Martin for their guidance and support. Special thanks to Dr. Xiaoliang Zhang who offered a tremendous amount of time answering my questions and elaborating on hardware/physics concepts. Thanks to classmates of the MSBI program for moral support and providing a leeway for taking breaks throughout the intense past months. Thanks to Dr. Peder Larson and Dr. Roland Krug for consultation of MR physics concepts. The members of the lab group working on this project deserve significant recognition as without them, this project would not have reached the stage that it has; I'm deeply grateful to Bradford Thorne, Jeffrey Yang, and Dr. Prasheel Lillaney. Finally, I'd like to acknowledge my family for support and providing me with the education that I have.

Integrating Resonator to Catheters for MR-Guided Interventional Radiology

Jeffrey Hu

Abstract

Stroke and cardiovascular disease are major health threats in the United States. Treatment is typically done under X-ray fluoroscopy but MR imaging could provide physiological information and does not have ionizing radiation. An issue with MR is that tools have to be compatible in a magnetic field environment. Hence, the aim is to build an RC with satisfactory tip visualization at various orientations. It will be utilized in a stroke model involving swine where the catheter will be inserted in the femoral artery up to the carotid. There will also be testing the accuracy of the electromagnetic simulation software XFdtd.

A unique material, pyralux (by Dupont), was processed with photolithography to etch the design. The resonators were wrapped around catheters and tuning was done to achieve the proper resonant frequency for 3.0 T and 1.5 T MR scanners. Scans were made with vascular phantoms and mainly MRA (TOF GRE) protocols. Catheters were oriented perpendicular or parallel to the B0 magnetic field. OsiriX and MS excel were used to calculate the SNR of the catheter relative to the background.

Increasing flip angle, starting from 5 degrees and ending at 90 degrees, decreases the SNR and stronger signal is achieved at 1.5T than 3.0T with these parameters. There is not a significant different between SNR with the perpendicular and parallel orientations in the 3.0T. XFdtd successfully demonstrated the relationship between frequency, capacitance, and inductance with a single coil model but not with the double helix. A clot was successfully induced in the femoral artery of a pig and temperature mapping shows insignificant heating hazards.

The goal of the resonator is to visualize the tip, so wider bandwidth would be useful to account for frequency shifts caused by magnetic field disturbances. While choosing the ROI for analysis, selection was based off covering the catheter width and choosing the background such that any artifacts can be accounted for. Although the same TOF GRE sequence in previous successful cases were used, the new sequences tested this year were variable so they were not included in analysis.

From this study, it is shown that the resonator has similar SNR regardless of orientation in the GE 3.0 T scanner. It would be most beneficial to use low flip angles and currently the 1.5 T scanner.

Table of Contents

List of Figures:

List of Tables:

Introduction

Typical Modalities

Public health threats such as ischemic stroke, brain aneurysm, and atherosclerosis are major causes of death and disability in the United States. Image-guided endovascular interventions is a growing field as studies continue to demonstrate similar efficacy and lower morbidity when compared to traditional surgical techniques.[1-5] For cardiac applications, such as quantifying ejection fraction and wall motion score, echocardiography is the most commonly used clinical method. However, it is associated with inability to differentiate dyskinetic from hypokinetic myocardium.[6-8] The gold standard for diagnosis and treatment is currently under x-ray fluoroscopic guidance, but even this modality has its disadvantages. Prolonged navigation can result in increased radiation dose to the patient and interventionist when using x-ray fluoroscopic visualization, as well as thrombus formation and use of increased volume of exogenous contrast.[9-18]

MRI

Unlike other modalities, magnetic resonance imaging (MRI) provides quantitative functional and structural information.[23,24] Previously, low spatial and temporal resolution have made the modality unattractive but recent development aims to reverse that trend.[19,20] The development of wide-bore and open MR scanners provides a dimension of access to the patient that was previously not possible. With the open MR environment, interventional procedures became feasible for a variety of applications.[19] For example, clinical MRI studies demonstrated the impairment in radial, circumferential and longitudinal strain in ischemic myocardium.[21-23] Investigators found that MRI had higher sensitivity and specificity than 2D strain echocardiography in patients with acute myocardial infarctions[24] and scar.[25] Furthermore, contrast enhanced MRI can delineate patchy myocardial infarct in patients[26] and animals.[27-29]

MR perfusion and thermometry allow for monitoring the effects of procedures such as thermal and cryo-ablations. For instance, while treating an acute ischemic stroke caused by thromboembolic occlusion of a cerebral artery, it is possible to visualize the ischemic penumbra (via perfusion) surrounding the core infarct (via diffusion) such that a clinical determination can be made as to whether to reopen an occluded artery while the intervention is being executed. This intra-procedural evaluation of tissue damage could prevent hemorrhage upon reopening an artery into brain tissue that is already infarcted.[30]

Steering

The majority of endovascular interventions require the use of a guidewire, a small profile, flexible metal wire with a hydrophilic coating. Providing a stable track, a catheter is then introduced over the wire.[31] Because the guidewires are relatively rigid compared to the vessel walls, they can cause vessel wall dissection, perforation, and hemorrhage.[9-18] Furthermore, with specific applications such as treatment of an aneurysm, catheter steering is difficult when the neck is oriented 90 degrees to the parent vessel.[32,33] In fact, one of the challenges of endovascular interventional procedures is to remotely direct the catheter tip into tiny blood vessel branches. Conventionally, development of catheter materials, tip geometries, and manual skill of the practitioner have been used to address this issue.[34]

MARC

To tackle the catheter navigation issue, copper coils (orthogonal helical shaped and saddle-shaped) have been mounted on the catheter tip. They were tested on a 1.5 T scanner where steady state free precession(SSFP) was empirically judged to be most suitable.[35] The coils, when energized, create a miniature magnetic field, resulting in an observable artifact at the catheter tip. When no current runs through the tip, the minimal artifact allows high-resolution local tissue imaging.[36] Deflection of the magnetically-assisted remote control (MARC) catheter

tip occurs when the magnetic field generated by the coil is not parallel to B0.[37] For three-dimensional deflections, magnetic moments in three-dimensional space are necessary.[38] However, the electric current required to generate these magnetic moments also generate enough heat through resistive dissipation; this causes temperatures unsafe for blood or vascular walls. Heating could also occur in the wires within the lumen of the catheter due to the B0 field coupling with the radiofrequency magnetic fields.[39-41]

Tip Visualization

Accordingly, tip visualization has to be achieved and this has been difficult due to the MR environment. Several techniques have been proposed to highlight the instrument tip, thus enabling the precise positioning of the instrument.[42] Heavy-metal compound markers at the catheter tip are typically used for tip visualization in x-ray fluoroscopy. In MRI however, such markers may either disrupt the image or in the case of markers with ferromagnetic properties, be unsafe. Therefore, alternative visualization methods such as passive and active catheter tip tracking have been developed.[43-45]

Passive position monitoring techniques are confronted with the challenge to generate sufficient contrast between the instrument and surrounding anatomy.[20] They also do not deliver coordinates that are required for fast and automated device localization. However, they are cost effective and easy to implement. A common approach is to embed a coating containing paramagnetic particles onto the device. This locally distorts the homogenous static magnetic B0 field.[42] Active guidance relies on incorporating a miniature rf coil into the instrument. It provides superior visualization and allows for automatic tracking of absolute coordinates using small receive coils at the tip with the coaxial cable connected to the scanner. Another method is based on local magnetic fields generated by DC fed conducting structures. Subtraction of MR images with and without DC yields images from which device location can be extracted.[42]

A method that has taken off and is proving to be feasible is the application of resonant circuits. The low levels of current supplied to the resonator would aid in this undertaking. If tuned to the Larmor frequency, the resonator substantially enhances the excitation angle in and adjacent to the fiducial coil, and locally increases the sensitivity of the receive coil.[46] RCs implemented on interventional instruments produce intense local signal enhancement on gradient and spin echo sequences after small tip excitation. The transmit coil couples to the fiducial coil, locally enhancing the B1 field and thus enhancing excitation angle in directly adjacent surroundings of the fiducial coil. A major issue however is that current markers lose signal enhancement for certain orientations.[20] Hence, our goal is to create a catheter-compatible resonator that can be visualized regardless of orientation to the inherent B0 field.

Materials and Methods

Physics

In previous models, wire was used, but in this study, a resonator was built via photolithography to achieve a smaller profile which is a staple in endovascular procedures.

Photolithography (Figure 1) results in a resonator a polyimide layer of 0.025 mm thick, and copper layers of 0.018 mm thick. It was tuned to the Larmor frequency on a 3.0 T (128 MHz) GE scanner and on a 1.5 T (63.9 MHz) Phillips Scanner. Relevant theory and equations are important to calculations of resonant frequency. Resonant frequency is calculated via

$$f_0 = \frac{\omega_0}{2\pi} = \frac{1}{2\pi\sqrt{LC}} \qquad (1)$$

where f_0 represents resonant frequency, ω_0 represents angular frequency, L is the inductance (Henrys) which is calculated via the physical properties of the coil, and C is the capacitance (in picofarads). Q factor determines the sensitivity to the surrounding environment. It is defined by

$$Q = \frac{1}{R}\sqrt{\frac{L}{C}} = \frac{\omega_0 L}{R} \qquad (2)$$

where R is resistance.

In regards to simulations, a relationship between 2 frequencies and 2 capacitance values will be useful.

$$f1 / f2 = \sqrt{} C2 / \sqrt{}C1 \qquad (3)$$

The resonator model proposed is a single LC double helix with each helix being orthogonal to the other (Figure 2). The perpendicular orientation decouples the circuits. Also, the said design is independent of catheter orientation with regard to the B0 field direction.[46] The excitation of a single wound RC depends strongly on its degree of coupling with the B1 excitation field. Thus, visualization of a RC depends on the orientation of the coil surface axis to the B1 field direction. If the patient is oriented in the z-axis, and there is flux going through a orthogonal surface, a small flip angle excitation, such as 5 degrees, results in a substantially higher excitation in the fiducial surroundings.[20]

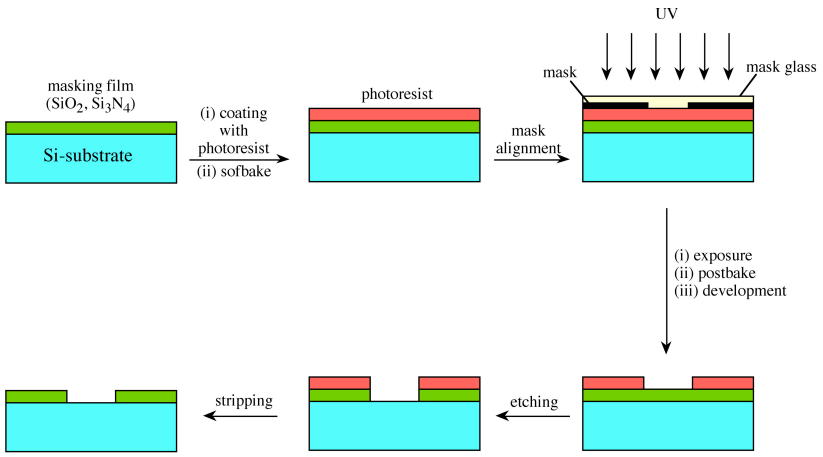

Figure 1: Photolithography Process. Coat copper (green layer) and polyimide(substrate) with photoresist. Align the photomask to protected regions. Apply UV light. Develop with sodium carbonate. Etch out the remaining copper with ammonium persulfate. Strip the remaining photo resist. Image from cnx.org 2015.

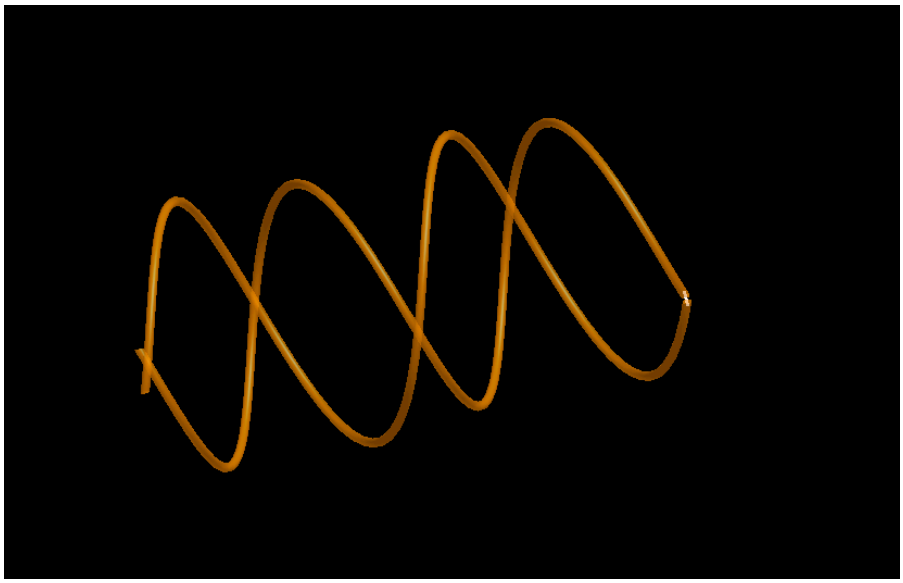

Figure 2: Double helix modeled in electromagnetic simulation software XFdtd. Parameters were adjusted to reflect the physical model and helices were oriented perpendicular to each other. Copper helices do not touch. Conductive wire completes the circuit at one end while a combination of the voltage source/capacitor completes the circuit at the other end.

Building the Resonator

The material used in the study is pyralux, which is composed of polyimide (dielectric material) sandwiched between a layer of copper. The process starts with thoroughly cleaning the working surface and substrate with isopropyl alcohol. A negative photoresist was laminated to the substrate. The photoresist is sensitive to traditional lighting so it is imperative for the process to be performed under a controlled environment. The process was repeated on the other side. A photomask in conjunction with a negative photoresist, contains the inverse of the pattern to be transferred. 2 photomasks were aligned (1 for each side of the material) and the product was UV exposed under a vacuum. UV light causes the negative resist to become polymerized, making it more difficult to dissolve. The pyralux was then placed in a developer solution (sodium carbonate) which removes the unexposed portions. 11% weight/volume of ammonium persulfate is used to remove the layers of substrate not protected by photoresist, otherwise known as the copper. The substrate was then placed in a stripper solution which alters the resist so that it no longer adheres to the substrate, thereby revealing the protected copper (Figure 3).

Ultimately, the resonators consisted of a capacitor section (copper-dielectric polyimide-copper) and an inductor section (just the polyimide). They were cut out by hand from the pyralux material.

Figure 3: Completed resonators on the pyralux sheet. One leg from the apex is the capacitance section where the squares incrementally change the capacitance. The other leg is the inductance section.

Tuning

The resonators were wrapped around a catheter (generously provided by Penumbra) with outer radii of 0.087" and inner radii of 0.084" (Figure 4) and the circuit was completed via conductive silver epoxy. The resonator was tuned in water using a network analyzer. Water was used to achieve the same permittivity as in the scan environment (the catheter will be flushed with water). Initially, only capacitance was adjusted by completing the circuit at various sections of the capacitor side of the resonator. The capacitor strip had a number of squares where each square would add/reduce the capacitance in increments. In later steps of the experiments, inductance was manipulated by adjusting the thickness of the polyimide, which is inversely proportional to the capacitance.

Figure 4: Manually cut out resonators wrapped around catheter with outer radii of 0.087". Copper layers do not touch and circuit was completed via silver epoxy.

Simulations

To aid in this process, the model was simulated via electromagnetic simulation software XFdtd by Remcom. The software facilitates a realistic environment for determining resonant frequency and quality factor (Q), which would be the variable for determining strength of the signal.[42] Simulating the entire MRI marker enables precise estimation of electrical properties as well as the impact within the MR environment. As the software is relatively new, a simple single loop coil design was built to confirm the validity of the software. A schematic depiction of the catheter was included for representational purposes only, so electromagnetic properties for the catheter were not included. In order to construct the coil, a cylinder with inner radii and outer radii parameters had to be constructed. With a series of rectangular block subtractions, the desired single loop coil was achieved (Figure 5).

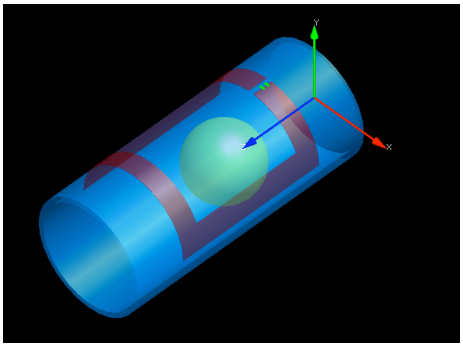

Figure 5: Single loop coil made out of rectangular modeled copper wire. A series of rectangular cuts had to performed in order to achieve desired design. Phantom placed in the center. Circuit completed via capacitor and power source (represented in green).

Modeling the double helix was more complicated as many parameters (Table 1) had to be adjusted and were dependent on each other. In addition, the copper helices should not touch (Figure 6), otherwise there would be a short circuit. Rather, the circuit was completed via an inductive wire.

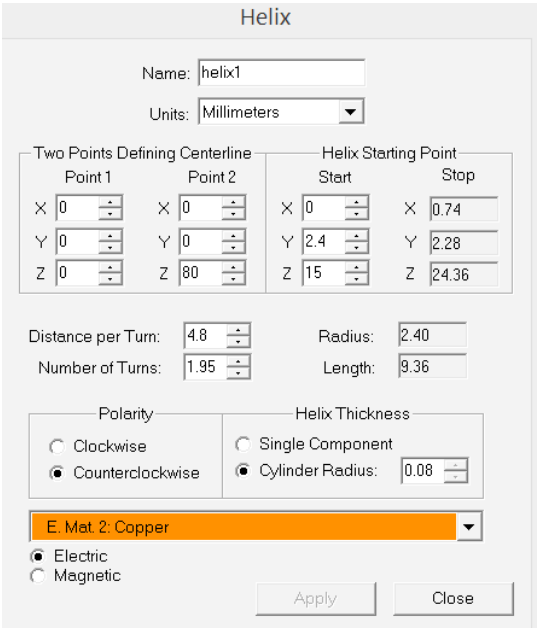

Table 1: The parameter of one helix of the double helix model via XFdtd. Parameters of note are the distance per turn and number of turns (which affect inductance). Cylinder radius is the radius of the wire itself.

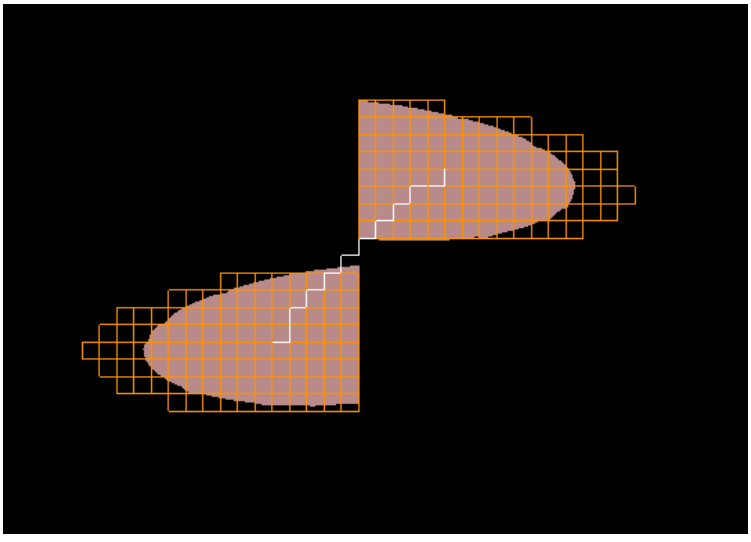

Figure 6: Double helix in mesh mode. The copper wires do not touch. The circuit is completed via conductive wire.

After modeling, a mesh has to be established for accuracy in calculations. It consisted of a grid of rectangles with user-controlled dimensions. A smaller mesh would give greater accuracy but take up more storage and prolong calculations. Hence, it is preferred if a balance between the two are achieved. It is also of note that mesh dimension (in x,y,z axis) could be based on the geometry of the RC, so as to achieve efficiency between time and accuracy. As such, in an axis without little variation, a larger dimension could be used whereas with many variations, it is necessary to use a smaller dimension. In the simulations for the double helix, a suitable size mesh was established such that at least 9 full voxels could fit into the helix as seen from the yz plane (Figure 7).

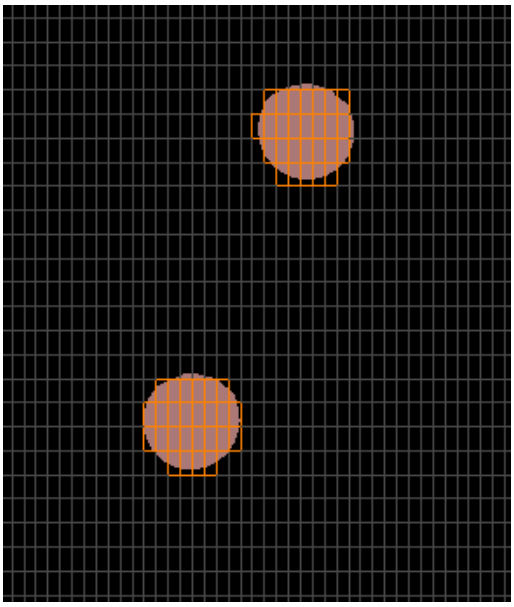

Figure 7: Double helix as seen in the YZ plane in mesh mode. A mesh size is chosen such that at least 9 rectangles fill each helical wire.

Given that helix wire had a radius of 0.08 mm, a mesh of 0.02 mm (x), 0.02 mm (y), 0.04 mm (z) was determined to be appropriate. A port is then established with varying resistance, but starting with 50 ohms (the standard for the software). A capacitor (which is the same tool as the port) is constructed as well and the capacitance is inputted. Simulation was particularly used to find inductance but there was not a direct method to calculate it from the geometry of the model. Hence, our chosen capacitance and desired resonant frequency were inputted to find the inductance. The software could input a voltage source thereby generating the s11 graph. This is to verify the resonant frequency and observe the Q factor. Resistance was then modified to vary the sensitivity of the peak and test the accuracy of the software. Of note is that the number of time steps were adjusted as well. In earlier simulation, the number of time steps was set to

10,000 so there wasn't enough calculations to get a meaningful plot. In later simulations, the time step was set to 100,000 which was sufficient.

Scan

The initial MR scan consisted of testing the efficacy of a novel guidewire by MARVIS inserted into a MR-safe catheter. Navigation was tested with an experienced and inexperienced user in which, poor visualization was seen in both cases. A cryogel abdominal aortic phantom (and other vascular phantoms) were used consisting of branching arteries of 30, 45, 60, and 75 degrees (Figure 8). It provides slippery walls and physiologically relevant vessel trajectories and diameters (6.4-22.2 mm). The phantom was placed in distilled water in a plastic bin with ½" vinyl tubing connected to the bin. A 5.3 mm introducer sheath was inserted into the tubing to mimic the size of a typical vascular access, although it simulated accessing from the upper extremity rather than the femoral artery.[47]

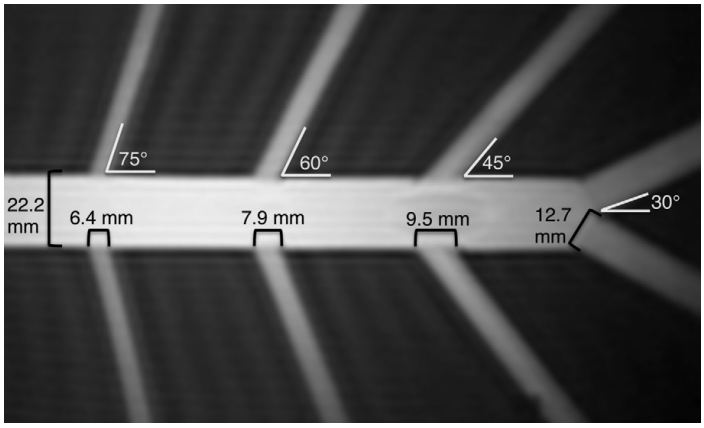

Figure 8: Abdominal phantom with various angles of branching arteries to simulate a realistic environment. Slippery walls and access from above do not simulate the actual environment however. Phantom was placed in distilled water and has an introducer sheath.

Subsequent scans involved the catheter with our integrated resonator. It was tested in an orientation perpendicular to the B0 in the 1.5 T in order to confirm results from a previous study in the Hetts lab. In the past, copper coil was used for visualization. Comparison was done to

see if there would be any difference with pyralux. Scans were then performed in the 3.0 T scanner in parallel and perpendicular orientation. Fast TOF GRE sequence was used with flip angles of 1,5,10,20, and 90 degrees. Data analysis was performed via selecting regions of interest for intensity and noise (background); the software used was Osirix.

Clinical Progress

Once simulations and actual construction of the catheter are complete, progress towards clinical value can commence. As the technology is still in an early stage, we used the RC in a pig model. Foreseeably, a stroke will be induced in the carotid artery and the catheter will be inserted under standard surgical procedure. Tip visualization at various orientations will be observed. If a clot is detected, it could be mechanically extracted or TPA (anticoagulant) could be injected. Temperature probes with fiber optics, were utilized to assess heating implications. The probes were placed in the lumen of the catheter, on the resonator, and in the water bath. MS Excel was used to enter the data and visualize the plot. To advance the goal of using the resonator in a stroke model, an artificial clot was induced by taking blood out of the pig, allowing it to coagulate, and injecting it back into the femoral artery.

Magnet Strength (Tesla) - Flip Angle	Intensity of Catheter	Intensity of Background	Ratio of Intensity of Catheter/Intensity of Background
1.50-1.00	880.54	43.24	20.36
1.50-5.00	845.88	47.54	17.79
1.50-10.00	635.73	41.21	15.43
1.50-20.00	347.22	30.49	11.39
1.50-90.00	245.95	62.68	3.92

Table 2: Intensity of catheter over intensity of background ratios for 1.5 Tesla, at varying flip angles and with catheter oriented perpendicular to B0. Regions of interest were chosen based on manual perception. Increasing flip angle decreases the ratio.

Results

SNR and Temperature

Using a typical MR-safe catheter, images were visually poor with the 3.0 T (Figure 9). SNR was not measured as a result. Integrating the resonator, satisfactory visualization in the 1.5T was achieved with the resonator perpendicular to the z axis. Given the relatively consistent temperature plot of MRA, one of the major MR protocols used in clinical cases[37], there does not seem to be any heating hazards (Figure 10). Signal intensities were calculated via selecting an roi inside the coil and background (noise). Using various flip angles, lower flip angles gave the highest SNR (Table 2). With the 3.0 T, visibly less satisfactory images were obtained and the SNR values corroborate that (Table 3).

Magnet Strength (Tesla) - Flip Angle	Intensity of Catheter	Intensity of Background	Ratio of Intensity of Catheter/Intensity of Background
3.00-5.00	20912.50	10733.73	1.95
3.00-90.00	9472.70	6826.99	1.39

Table 3: Intensity of catheter over intensity of background ratios for 3.0 Tesla, at varying flip angles and with catheter oriented perpendicular to B0. Regions of interested were chosen based on manual perception. Increasing flip angle typically decreases the ratio.

In addition, the resonator was tested in an orientation parallel to the z axis, in which similar SNR was achieved (Table 4).

Magnet Strength (Tesla) - Flip Angle	Intensity of Catheter	Intensity of Background	Ratio of Intensity of Catheter/Intensity of Background
3.00-1.00	5220.00	2713.74	1.92
3.00-5.00	15748.75	7611.05	2.07
3.00-10.00	20668.33	13556.19	1.52
3.00-90.00	8353.38	7346.67	1.14

Table 4: Intensity of catheter over intensity of background ratios for 3.0 Tesla, at varying flip angles and with catheter oriented parallel to B0. Regions of interested were chosen based on manual perception. Increasing flip angle typically decreases the ratio.

Though parameters needed to target 128 MHz were calculated, initial tests showed a frequency of 2 GHz. Manipulation of the polyimide's thickness and capacitance eventually achieved a value of 128 MHz but the attenuation was about -4db, which is not strong.

Figure 9: Poor visualization of the catheter and guidewire, without the resonator, in the abdominal phantom during timing test for experience and inexperienced user.

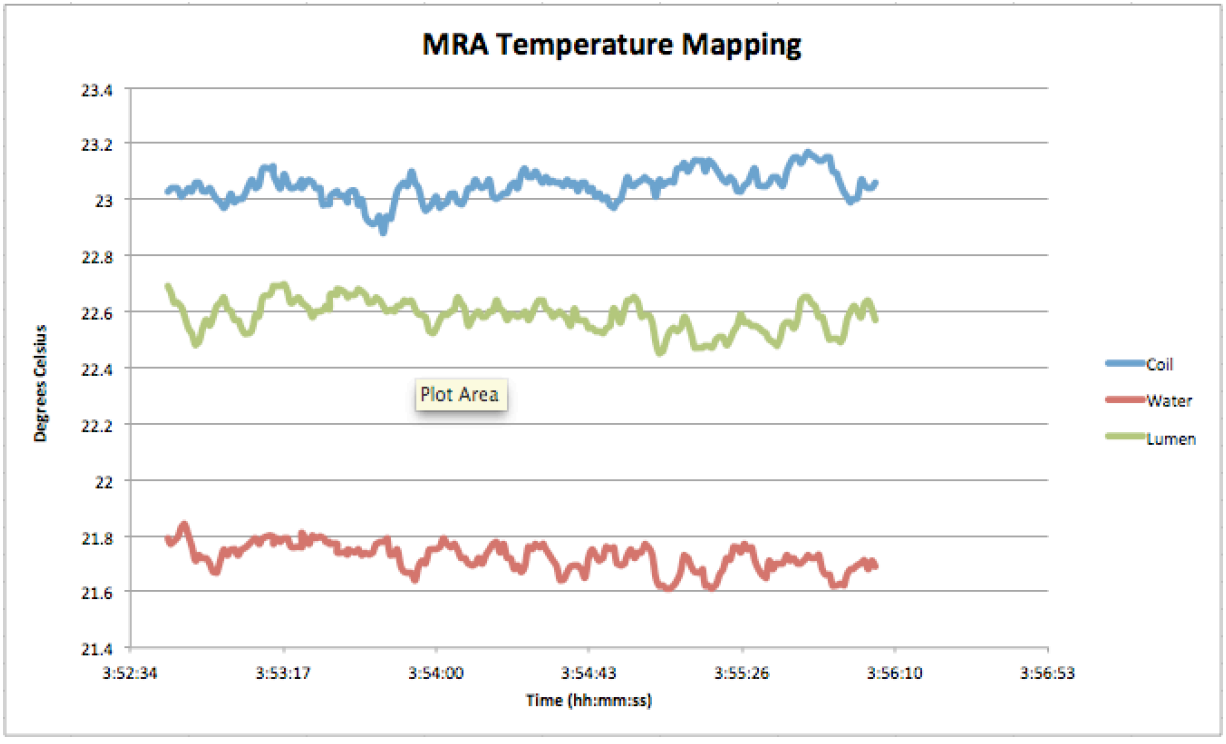

Figure 10: MRA temperature mapping with probes placed at different locations: on the coil, in the lumen, in the distilled water. Temperatures were relatively stable and do not seem to pose a heating hazard.

Calculations via XFdtd

With XFdtd, modeling of a single loop (Figure 5) accurately corresponded to equation (1). Setting the resistance of both capacitor and power source to 150 ohms, and arbitrarily setting the capacitance to 25 pf, a resonant frequency of 149.92 MHz was obtained (Figure 11).

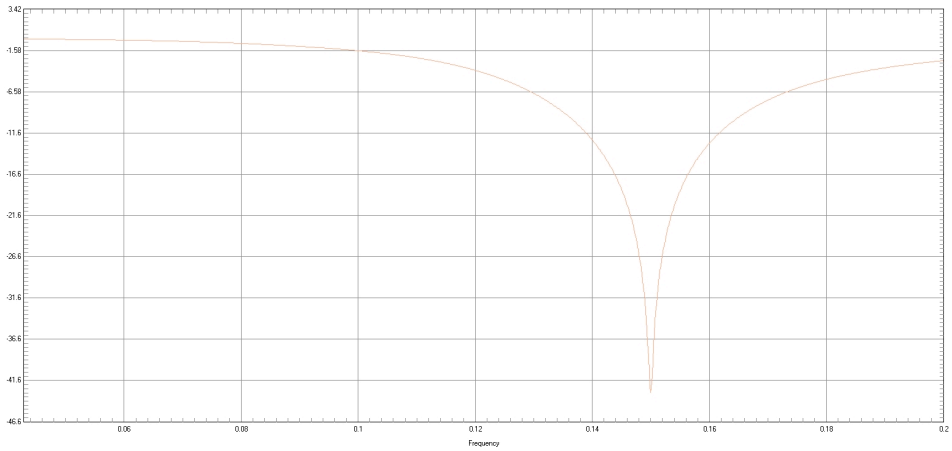

Figure 11: s11 plot simulated in XFdtd. Resistance of power source and capacitor set to 150 ohms. Capacitance was set to 25 pf. Resonant frequency of 149.92 MHz

Using equation (3) and assuming the target resonant frequency was 128 MHz, the capacitance should be changed to 34.30 pf. The resulting resonant frequency was 128.26 MHz (Figure 12) thereby confirming equation (1).

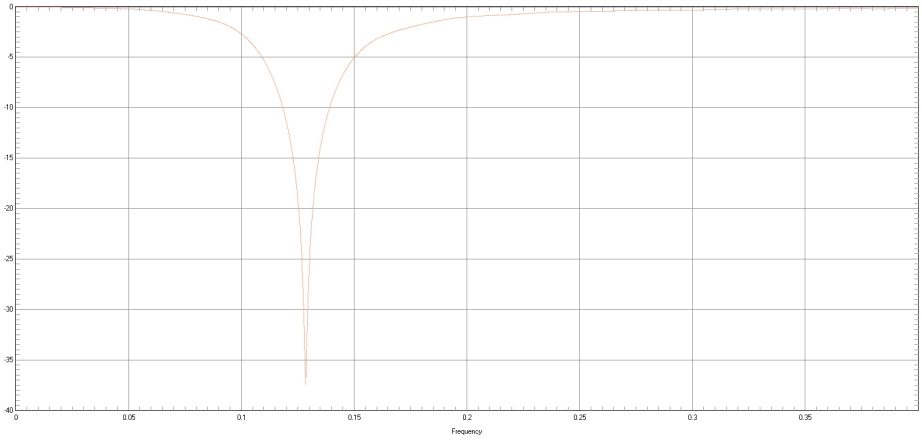

Figure 12: s11 plot simulated in XFdtd. Resistance of power source and capacitor set to 150 ohms. Capacitance was set to 34.30 pf. Resonant frequency of 128.26 MHz.

However, increasing resistance led to a visibly narrower peak and higher Q value. There also seems to be some instability along the fringes of the plot as resistance continues to increase (Figures 13.1-13.4). Values in the simulation were not applied to our actual resonator as a result. Finally, the clot procedure in the femoral artery was successfully performed under x-ray.

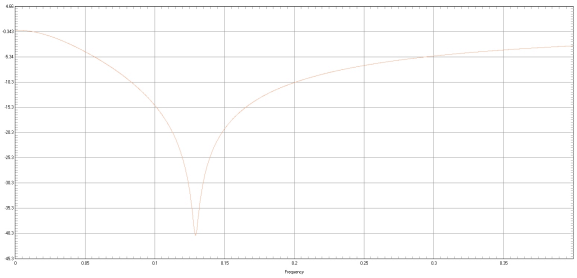

Figure 13.1: 25 ohms

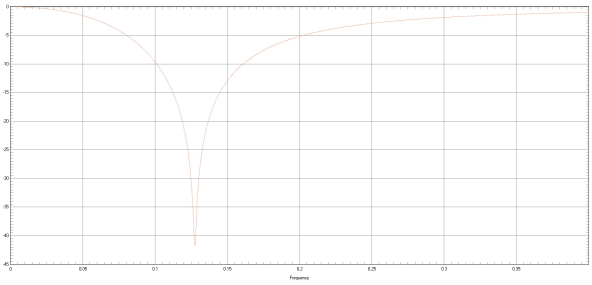

Figure 13.2: 50 ohms

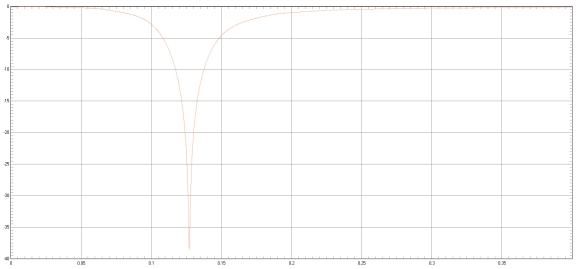

Figure 13.3: 150 ohms

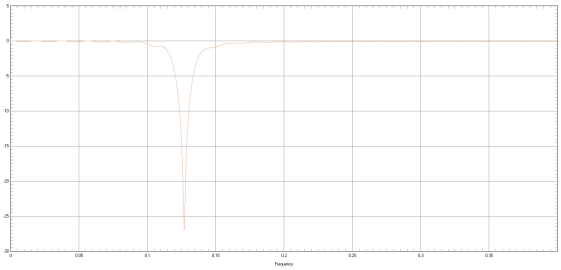

Figure 13.4: 500 ohms

Figures 13.1-13.4: Progression of adding resistance to the single loop coil (Resistance: 25, 50, 150, 500). Rather than having a wider bandwidth according to equation (2), the peak gets narrower and Q value appears to increase. Fringing appears on the boundaries with resistance of 500 ohms.

It was found that if there was a differential in resistance between the capacitor and voltage source, the s11 plot will look non-uniform (Figures 14.1, 14.2)

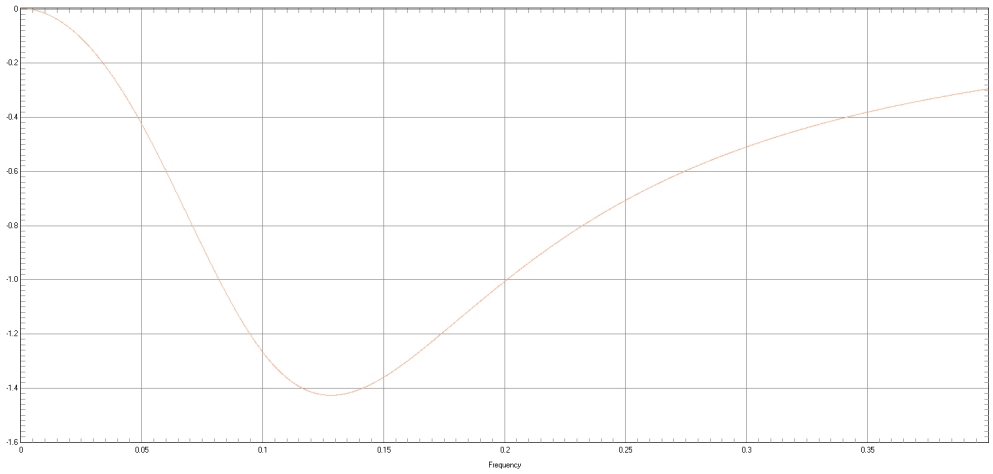

Figure 14.1: Resistance of capacitor is 25 ohms. Frequency is 128.01 MHz

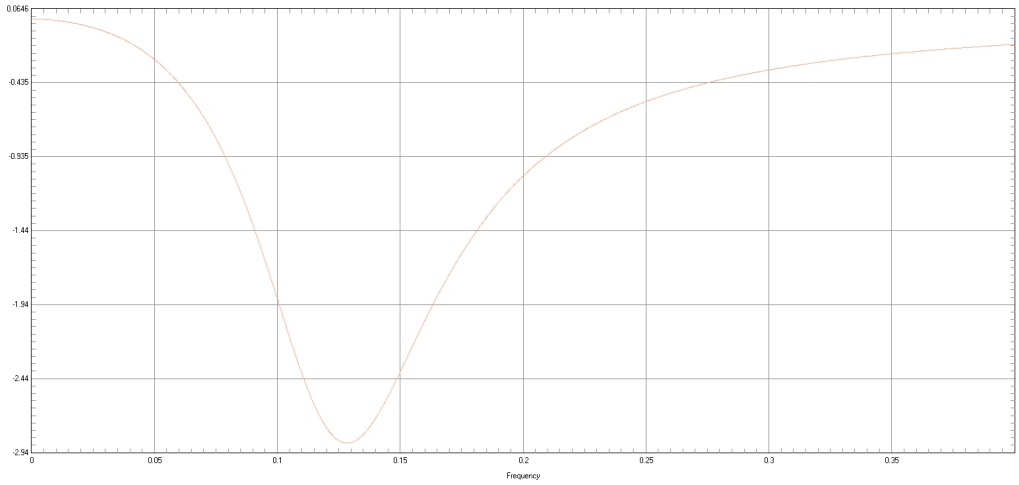

Figure 14.2: Resistance of capacitor is 50 ohms. Frequency is 128.50 MHz

Figures 14.1-14.2: s11 plot simulated via XFdtd to get a resonant frequency close to 128 MHz. Capacitance was kept at 34.3 pf. Resistance of power source was kept at 300 ohms while resistance of capacitor was varied to show incongruity of plot.

Applying equation (3) to the helical model, results are shown in Table 5.

Frequency(MHz)	Capacitance(pf)
150.00	25.00
127.00	28.50
123.80	30.00

Table 5: Varying capacitance of the double helix model to get resonant frequency.

Ultimately, the plot did cover 128 MHz but had a wide bandwidth and was not uniform

(Figure 15).

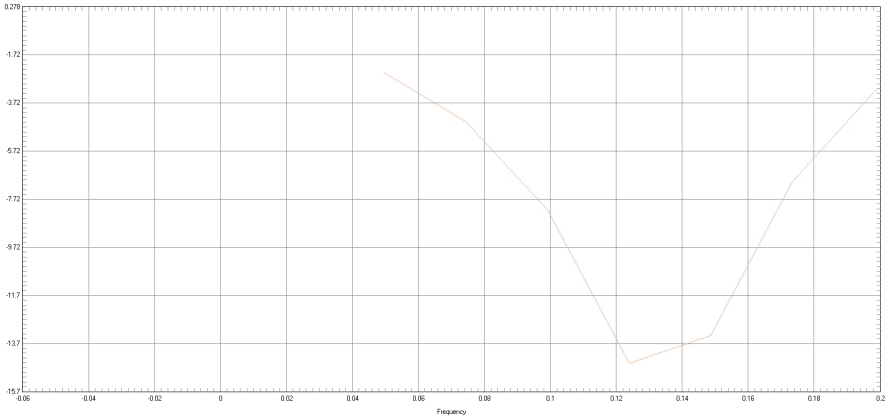

Figure 15: s11 plot of double helix, with resistance of source as 25 ohms. No resistance set for capacitance. Capacitance set to 28.19 pf as calculated from equation (3).

A plot resembling an s11 was only achieved by having no resistance on the capacitor. If any resistance were to be added onto the capacitor, the peak would be un-recognizable (Figure 16).

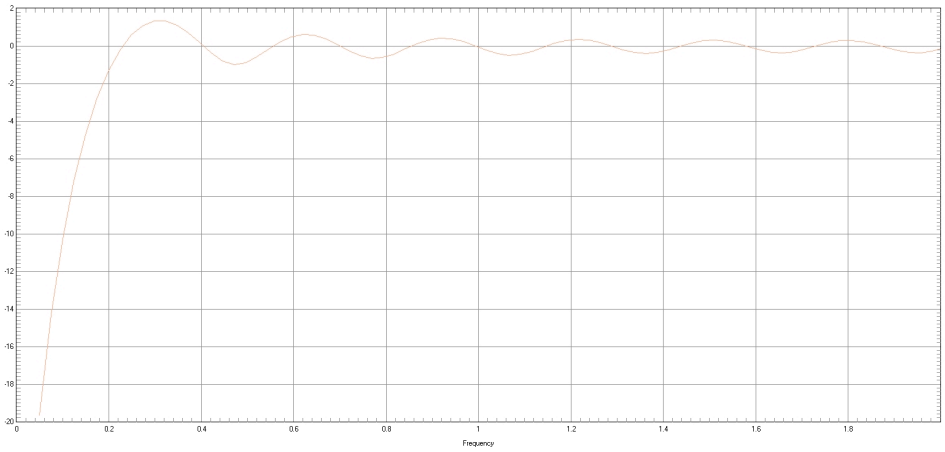

Figure 16: s11 plot with resistance of source as 50 ohms. 250 ohms resistance set for capacitance. Capacitance set to 50 pf.

Discussion

Loaded Case

As an objective of the study was to prioritize tip tracking, the Q factor does not have to be extremely high. High Q factor would result in higher sensitivity so that would be useful if the primary goal was to investigate surrounding tissue in detail. It should be noted that once the catheter is inserted in the vasculature, there will be magnetic field distortions, known as a loaded case. This can be due to hemoglobin or guide wires which can electromagnetically interact with the LC. Also, ultimately the catheter will become heat-shrunk. As a result, the resonant frequency as measured by simulation or network analyzer may shift. Compensation is performed by tuning in an environment with the same permittivity as our catheter, which we flush with water. However, it is challenging to simulate an iron-present blood environment until the actual scan. The discrepancy between controlled environments and the actual scan is also apparent via signal intensity. Although the peak may have great attenuation as shown in a network analyzer, it may not be a true assessment of the intensity within the scanner. This issue can only be resolved via trial and error with the actual scan as well. Having an s11 with a wider

bandwidth (Figure 17) hence would be useful. Even with a shift, the broad peak still covers the range and will resonate close to the Larmor frequency. Signal intensity will therefore not be lost.

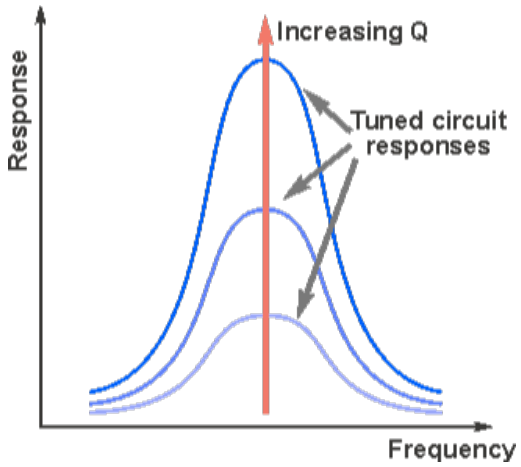

Figure 17: Representation of manipulating the Q factor. Increasing Q leads to a shorter bandwidth with higher peak. Image from Radio-electronics 2014.

Simulation Value Analysis

Assessing XFdtd, equation (1) is followed. Even in the double helix model, though resonant frequency is difficult to distinguish, it was still within range. In addition, applying equation (3), it was found that the software does keep the ratios the same. For example, using a frequency of 149.92 MHz (with 25 pf capacitance), and 128.76 MHz (with 34.3 pf), the ratios on both sides converge to 1.17. There seems to be widespread errors with equation (2) as from the software, resistance appears to be proportional to Q factor. Furthermore, having different resistance between the capacitor and power source alters the symmetry of the plot. This could be a software issue or this could instigate further investigation as to the validity. Finally, with the double helix model, adding any resistance to the capacitor would produce a plot that does not resemble an s11. In the actual resonator, there was no resistance attached to the capacitor so whether adding one would produce a conventional s11 plot is yet to be seen. Via simulation, the resistance can be experimented with to determine what is the ideal Q factor. However, it has

been seen in our study that XFdtd has complications regarding equation (2), so it would not be feasible to attempt it with that software.

Scan Parameters

The images with the 1.5 T in past years contrasted greatly with the images obtained with the same scanner in this study. The only difference was that the recent model was built out of paralux. Consultations with MR physicists were held and a possible reason could be due to image processing parameters. Parameters such as gray scale range and the dynamic range have to be consistent throughout scans. Another idea introduced was to have a manual prescan in which transmit gain was manipulated and the phantom was scanned first; it will then be introduced later. Along with the theme of consistency, scanning protocols were not that since the 1.5 T and 3.0 T were from different manufacturers. Suggested protocols were fast SPGR 3D, SSFSE, T1 FSE, T2 Flair, T2 FSE, DWI, and real-time Fiesta. However, the protocol decided on for most analysis is fast Time of Flight (TOF) GRE since that was the protocol used successfully in previous years. In addition, another sequence to investigate would be steady state free precession as it has been shown to have optimal spatial and temporal resolution for catheter-coil tip visualization.[48] Overall, quality of images may be improved by altering the parameters under which imaging is performed. A different imaging sequence may be used to determine if an increase in image quality and clarity is experienced.[49] Because tip visualization was still in its early stages, focus was mainly on whether the tip can be seen in the first place, regardless of standardization; hence, this was a flaw in study design.

Catheter Steering Methods

Several studies describe deflection of a guidewire with a magnetic tip under a guidance system consisting of two magnets positioned around the operating table. This system is limited due to the required use of the external magnetic system and separate, modified C-arm angiography

system for imaging. The use of large, movable, external magnets makes this system incompatible with real time MR imaging.[50-52] Another study demonstrated a catheter system that could achieve deflection by placing soft ferromagnetic spheres encased at the distal tip of a microcatheter. However, dipole-dipole interactions between spheres can lead to undesirable jumping displacement, preventing precise control of the catheter tip.[53] The issue with the MARC catheter is that electric currents required to generate desired magnetic moments can generate enough heat through resistive dissipation; this can cause temperatures unsafe for blood or vascular walls. Heating could also occur in the wires running down the lumen of the catheter due to field coupling with radiofrequency magnetic fields.[39-41] From several studies, it was found that the use of saline coolant and alumina to facilitate heat transfer are feasible options for a construct such as the MARC[54]. Further considerations for heating exist via the braiding of the catheters. RF induces heating of nitinol-braided during MR imaging however tungsten-braided showed potential safe use without SAR restrictions.[55] This suggests that further material development can be integrated in the resonator design to advance it toward clinical usage.

Temperature Regulations

The standards by the US Food and Drug Administration for recommended temperature rise should not exceed 1°C on or in the head and 2°C in the torso and extremities. While MR thermometry is within the capability of the scanner and could be used to obtain a general idea of temperatures within tissues, it is limited by interference from blood flow or other movement and by local distortion of the magnetic field by ferromagnetic components of the catheter;[56] hence, this was why fiber optics were used in this study. The temperature deviations in all 3 settings (bath, lumen, resonator) had a temperature change less than .2°C which validate the heating safety properties of the resonator.

Comparing Magnet Strength

Even though signal to noise ratio and spatial resolution is conventionally better in higher field strength, the 1.5 T had better visualization of the catheter in all cases.[57] This could be due to manufacturer differences or stronger magnetic field would actually not be suitable for this resonator. It was also observed that a smaller flip angle was sufficient to get the best SNR values. Overflipping would be excessive as evidenced by the appearance of artifacts. While calculating SNR, it should be noted that the roi size was not consistent throughout all measurements. The goal of getting a roi of a catheter was to cover the width such that areas of signal (and without) were covered (Figure 18).

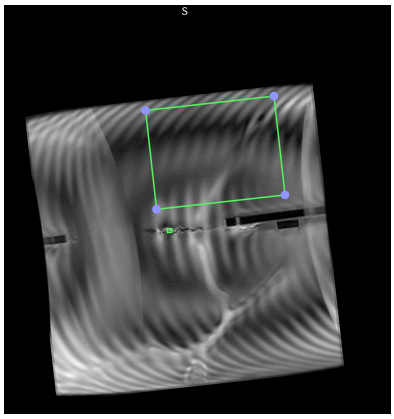

Figure 18: Fast TOF GRE (3.0 T) with flip angle of 90 degrees. Catheter is oriented perpendicular to magnetic field. Regions of interest are chosen such that they cover the entire width of the catheter and enough of the background such that varying intensities can be covered.

The goal of getting a roi of the background was to make sure it covered any ringing artifact or visible distortions. This method however is dependent on human judgment of accurate selections. Ultimately, the results do suggest that the resonator retains signal intensity regardless of orientation (with 3.0 T). Therefore, the future goal is to take the next step into clinical accessibility via implementation in a stroke model, specifically inducing a clot in the carotid artery and visualization of the resonator in this environment.

Further Steps

The orthogonal double helix coil design that was chosen has evidence of navigating tortuous vessels with satisfactory signal intensity. What can be explored however, is if this model does not operate as expected in the stroke setting, further RC designs can be proposed. One such example is a single RC with three faces. It will wrap around the catheter and no matter what orientation it is in, there will always be a loop having flux perpendicular to the subject. As the loops do not face each other, coupling is not expected but this instigates further investigation. In addition, the design can be compared for construction complexity and heating implications to better serve the clinical setting. With findings showing that the design in thos study does have good visualization for various orientations, steps are set for improving the attenuation and achieving greater signal intensity. Because there are issues automatically calculating inductance and finding the SNR via simulation, this part of the project may be dropped or reduced of significance. The values of interest that are necessary for this project to proceed can be substituted with the network analyzer.

Conclusion

The standard method of imaging endovascular intervention is with fluoroscopy, which yields concerns with dosage of contrast agents and radiation. In patients who are susceptible to such influences such as young children or pregnant women, the risks may not justify the benefit. Hence, an evolving field of using MR guidance has developed. This does come with MR constraints, which include limited patient access, insufficient assortment of compatible instruments, and difficult device visualization.[42] Various techniques to tackle the challenge have developed, but RCs seem to have gained the most traction. For endovascular procedures, the RCs can be implemented with catheters to achieve good visualization and low hazard to the patient. It is notable however, that some procedures involve navigating through tortuous

vessels. This causes a change of orientation with respect to the magnetic field and signal loss may occur. In this study, we proposed the usage of decoupled RCs aligned orthogonally to combat this issue. It has been shown that if the catheter is oriented parallel or perpendicular to the B0, signal intensity will not be lost.

When completely developed, the resonator would allow the interventionist to make treatment decision based on real-time MR-based physiological information, which is not a perk with x-ray guidance. Also, navigational speed is expected to be as fast as standard x-ray guidance. Adding to the time efficiency, especially related to the treatment of ischemic stroke, many treatment decisions are based on non invasive imaging before the intervention has started, such as perfusion or diffusion MR imaging. Consequently, the technology would allow differentiation of viable and nonviable brain tissue intraoperatively; this helps guide the interventionist as to which occluded arteries should be revascularized and which are more safely left occluded.

A major concern throughout the patient community is x-ray radiation. Especially with patients destined for multiple angiograms or young patients, exposure to the amount of radiation may actually result in overall greater risk. Successful development of MR safe endovascular catheters would eliminate ionizing radiation risks. As further progress of the resonator, photo lithography has reduced the overall profile as opposed to traditional wire, which is especially significant for applications in smaller vessels.[58]

From this study, it was shown that the resonator is visible with orientations parallel and perpendicular to the 3.0 T B0 magnetic field; the SNR values, which are based on the intensity of the resonator to the background noise, for respective flip angles confirm this. However, SNR values were greater in 1.5 T so this suggests the resonator is better suited for that scanner. In addition, temperature tests using fiber optics have not shown significant heating hazards and a

clot was successfully induced in the femoral artery of a pig; these are progressive steps for clinical relevance. Using the electromagnetic simulation software XFdtd, it was found that applications to the helical model were not viable, but useful information such as confirming the resonant frequency (relative to capacitance and inductance) can still be applied to a simple single coil. Overall, the resonator has achieved milestone targets and will soon be applied to an animal stroke model for the eventual goal of achieving clinical significance.

References

1. Becker DM, Philbrick JT, Selby JB. Inferior vena cava filters. Indications, safety, effectiveness. Arch Intern Med 1992;152:1985-94.

2. Hoffman SN, TenBrook JA, Wolf MP, Pauker SG, Salem DN, Wong JB. A meta-analysis of randomized controlled trials comparing coronary artery bypass graft with percutaneous transluminal coronary angioplasty: one- to eight-year outcomes. J Am Coll Cardiol 2003;41:1293-304.

3. Razavi MK, Hwang G, Jahed A, Modanlou S, Chen B. Abdominal myomectomy versus uterine fibroid embolization in the treatment of symptomatic uterine leiomyomas. AJR Am J Roentgenol 2003;180:1571-5.

4. Endovascular versus surgical treatment in patients with carotid stenosis in the Carotid and Vertebral Artery Transluminal Angioplasty Study (CAVATAS): a randomised trial. Lancet 2001;357:1729-37.

5. Molyneux AJ, Kerr RS, Yu LM, et al. International subarachnoid aneurysm trial (ISAT) of neurosurgical clipping versus endovascular coiling in 2143 patients with ruptured intracranial aneurysms: a randomised comparison of effects on survival, dependency, seizures, rebleeding, subgroups, and aneurysm occlusion. Lancet 2005;366:809-17.

6. Reisner SA, Lysyansky P, Agmon Y, Mutlak D, Lessick J, Friedman Z. Global longitudinal strain: a novel index of left ventricular systolic function. J Am Soc Echocardiogr 2004;17:630-3.

7. Lang RM, Bierig M, Devereux RB, et al. Recommendations for chamber quantification: a report from the American Society of Echocardiography's Guidelines and Standards Committee and the Chamber Quantification Writing Group, developed in conjunction with the European Association of Echocardiography, a branch of the European Society of Cardiology. J Am Soc Echocardiogr 2005;18:1440-63.

8. Moller JE, Hillis GS, Oh JK, Reeder GS, Gersh BJ, Pellikka PA. Wall motion score index and ejection fraction for risk stratification after acute myocardial infarction. Am Heart J 2006;151:419-25.

9. Lin PH, Bush RL, Peden EK, et al. Carotid artery stenting with neuroprotection: assessing the learning curve and treatment outcome. Am J Surg 2005;190:850-7.

10. Balduf LM, Langsfeld M, Marek JM, Tullis MJ, Kasirajan K, Matteson B. Complication rates of diagnostic angiography performed by vascular surgeons. Vasc Endovascular Surg 2002;36:439-45.

11. Ross IB, Dhillon GS. Complications of endovascular treatment of cerebral aneurysms. Surg Neurol 2005;64:12-8; discussion 8-9.

12. Young N, Chi KK, Ajaka J, McKay L, O'Neill D, Wong KP. Complications with outpatient angiography and interventional procedures. Cardiovasc Intervent Radiol 2002;25:123-6.

13. Gunning MG, Williams IL, Jewitt DE, Shah AM, Wainwright RJ, Thomas MR. Coronary artery perforation during percutaneous intervention: incidence and outcome. Heart 2002;88:495-8.

14. Fukutomi T, Suzuki T, Popma JJ, et al. Early and late clinical outcomes following coronary perforation in patients undergoing percutaneous coronary intervention. Circ J 2002;66:349-56.

15. Fasseas P, Orford JL, Panetta CJ, et al. Incidence, correlates, management, and clinical outcome of coronary perforation: analysis of 16,298 procedures. Am Heart J 2004;147:140-5.

16. Gruberg L, Pinnow E, Flood R, et al. Incidence, management, and outcome of coronary artery perforation during percutaneous coronary intervention. Am J Cardiol 2000;86:680-2, A8.

17. Willinsky RA, Taylor SM, TerBrugge K, Farb RI, Tomlinson G, Montanera W. Neurologic complications of cerebral angiography: prospective analysis of 2,899 procedures and review of the literature. Radiology 2003;227:522-8.

18. Gradinscak DJ, Young N, Jones Y, O'Neil D, Sindhusake D. Risks of outpatient angiography and interventional procedures: a prospective study. AJR Am J Roentgenol 2004;183:377-81.

19. Hetts SW, Saeed M, Martin AJ, et al. Endovascular catheter for magnetic navigation under MR imaging guidance: evaluation of safety in vivo at 1.5T. AJNR Am J Neuroradiol 2013;34:2083-91.

20. Kuehne T, Fahrig R, Butts K. Pair of resonant fiducial markers for localization of endovascular catheters at all catheter orientations. J Magn Reson Imaging 2003;17:620-4.

21. Croisille P, Moore CC, Judd RM, et al. Differentiation of viable and nonviable myocardium by the use of three-dimensional tagged MRI in 2-day-old reperfused canine infarcts. Circulation 1999;99:284-91.

22. Marcus JT, Gotte MJ, Van Rossum AC, et al. Myocardial function in infarcted and remote regions early after infarction in man: assessment by magnetic resonance tagging and strain analysis. Magn Reson Med 1997;38:803-10.

23. Gotte MJ, van Rossum AC, Twisk JWR, Kuijer JPA, Marcus JT, Visser CA. Quantification of regional contractile function after infarction: strain analysis superior to wall thickening analysis in discriminating infarct from remote myocardium. J Am Coll Cardiol 2001;37:808-17.

24. Migrino RQ, Zhu X, Pajewski N, Brahmbhatt T, Hoffmann R, Zhao M. Assessment of segmental myocardial viability using regional 2-dimensional strain echocardiography. J Am Soc Echocardiogr 2007;20:342-51.

25. Rosendahl L, Blomstrand P, Brudin L, Todt T, Engvall JE. Longitudinal peak strain detects a smaller risk area than visual assessment of wall motion in acute myocardial infarction. Cardiovasc Ultrasound 2010;8:2.

26. Choi JW, Gibson CM, Murphy SA, Davidson CJ, Kim RJ, Ricciardi MJ. Myonecrosis following stent placement: association between impaired TIMI myocardial perfusion grade and MRI visualization of microinfarction. Catheter Cardiovasc Interv 2004;61:472-6.

27. Saeed M, Hetts SW, Ursell PC, Do L, Kolli KP, Wilson MW. Evaluation of the acute effects of distal coronary microembolization using multidetector computed tomography and magnetic resonance imaging. Magn Reson Med 2012;67:1747-57.

28. Carlsson M, Saloner D, Martin AJ, Ursell PC, Saeed M. Heterogeneous microinfarcts caused by coronary microemboli: evaluation with multidetector CT and MR imaging in a swine model. Radiology 2010;254:718-28.

29. Breuckmann F, Nassenstein K, Bucher C, et al. Systematic analysis of functional and structural changes after coronary microembolization: a cardiac magnetic resonance imaging study. JACC Cardiovasc Imaging 2009;2:121-30.

30. Gonzalez RG. Imaging-guided acute ischemic stroke therapy: From "time is brain" to "physiology is brain". AJNR Am J Neuroradiol 2006;27:728-35.

31. Seldinger SI. Catheter replacement of the needle in percutaneous arteriography; a new technique. Acta radiol 1953;39:368-76.

32. McDougall CG, Halbach VV, Dowd CF, Higashida RT, Larsen DW, Hieshima GB. Causes and management of aneurysmal hemorrhage occurring during embolization with Guglielmi detachable coils. J Neurosurg 1998;89:87-92.

33. Vinuela F, Duckwiler G, Mawad M. Guglielmi detachable coil embolization of acute intracranial aneurysm: perioperative anatomical and clinical outcome in 403 patients. J Neurosurg 1997;86:475-82.

34. Roberts TP, Hassenzahl WV, Hetts SW, Arenson RL. Remote control of catheter tip deflection: an opportunity for interventional MRI. Magn Reson Med 2002;48:1091-5.

35. Wilson MW, Martin AB, Lillaney P, et al. Magnetic catheter manipulation in the interventional MR imaging environment. J Vasc Interv Radiol 2013;24:885-91.

36. Sincic RS, Caton CJ, Lillaney P, et al. System architecture for a magnetically guided endovascular microcatheter. Biomed Microdevices 2014;16:97-106.

37. Martin AJ, Lillaney P, Saeed M, et al. Digital subtraction MR angiography roadmapping for magnetic steerable catheter tracking. J Magn Reson Imaging 2015;41:1157-62.

38. Settecase F, Sussman MS, Wilson MW, et al. Magnetically-assisted remote control (MARC) steering of endovascular catheters for interventional MRI: a model for deflection and design implications. Med Phys 2007;34:3135-42.

39. Konings MK, Bartels LW, Smits HF, Bakker CJ. Heating around intravascular guidewires by resonating RF waves. J Magn Reson Imaging 2000;12:79-85.

40. Dempsey MF, Condon B, Hadley DM. Investigation of the factors responsible for burns during MRI. J Magn Reson Imaging 2001;13:627-31.

41. Nitz WR, Oppelt A, Renz W, Manke C, Lenhart M, Link J. On the heating of linear conductive structures as guide wires and catheters in interventional MRI. J Magn Reson Imaging 2001;13:105-14.

42. Kaiser M, Detert M, Rube MA, et al. Resonant marker design and fabrication techniques for device visualization during interventional magnetic resonance imaging. Biomed Tech (Berl) 2015;60:89-103.

43. Hillenbrand CM, Elgort DR, Wong EY, et al. Active device tracking and high-resolution intravascular MRI using a novel catheter-based, opposed-solenoid phased array coil. Magn Reson Med 2004;51:668-75.

44. Zuehlsdorff S, Umathum R, Volz S, et al. MR coil design for simultaneous tip tracking and curvature delineation of a catheter. Magn Reson Med 2004;52:214-8.

45. Miquel ME, Hegde S, Muthurangu V, et al. Visualization and tracking of an inflatable balloon catheter using SSFP in a flow phantom and in the heart and great vessels of patients. Magn Reson Med 2004;51:988-95.

46. Kuehne T, Weiss S, Brinkert F, et al. Catheter visualization with resonant markers at MR imaging-guided deployment of endovascular stents in swine. Radiology 2004;233:774-80.

47. Losey AD, Lillaney P, Martin AJ, et al. Magnetically assisted remote-controlled endovascular catheter for interventional MR imaging: in vitro navigation at 1.5 T versus X-ray fluoroscopy. Radiology 2014;271:862-9.

48. Settecase F, Hetts SW, Martin AJ, et al. RF Heating of MRI-Assisted Catheter Steering Coils for Interventional MRI. Acad Radiol 2011;18:277-85.

49. Hetts SW, Saeed M, Martin A, et al. Magnetically-Assisted Remote Controlled Microcatheter Tip Deflection under Magnetic Resonance Imaging. J Vis Exp 2013.

50. Krings T, Finney J, Niggemann P, et al. Magnetic versus manual guidewire manipulation in neuroradiology: in vitro results. Neuroradiology 2006;48:394-401.

51. Ramcharitar S, Patterson MS, van Geuns RJ, van Meighem C, Serruys PW. Technology Insight: magnetic navigation in coronary interventions. Nat Clin Pract Cardiovasc Med 2008;5:148-56.

52. Schiemann M, Killmann R, Kleen M, Abolmaali N, Finney J, Vogl TJ. Vascular guide wire navigation with a magnetic guidance system: experimental results in a phantom. Radiology 2004;232:475-81.

53. Gosselin FP, Lalande V, Martel S. Characterization of the deflections of a catheter steered using a magnetic resonance imaging system. Med Phys 2011;38:4994-5002.

54. Bernhardt A, Wilson MW, Settecase F, et al. Steerable catheter microcoils for interventional MRI reducing resistive heating. Acad Radiol 2011;18:270-6.

55. Losey AD, Lillaney P, Martin AJ, et al. Safety of retained microcatheters: an evaluation of radiofrequency heating in endovascular microcatheters with nitinol, tungsten, and polyetheretherketone braiding at 1.5 T and 3 T. J Neurointerv Surg 2014;6:314-9.

56. Muller L, Saeed M, Wilson MW, Hetts SW. Remote control catheter navigation: options for guidance under MRI. J Cardiovasc Magn Reson 2012;14:33.

57. Blamire AM. The technology of MRI--the next 10 years? Br J Radiol 2008;81:601-17.

58. Moftakhar P, Lillaney P, Losey AD, et al. New-Generation Laser-lithographed Dual-Axis Magnetically Assisted Remote-controlled Endovascular Catheter for Interventional MR Imaging: In Vitro Multiplanar Navigation at 1.5 T and 3 T versus X-ray Fluoroscopy. Radiology 2015:142648.

Publishing Agreement

It is the policy of the University to encourage the distribution of all theses, dissertations, and manuscripts copies of all UCSF theses, dissertations, and manuscripts will be routed to the library via the Graduate Division. The library will make all theses, dissertations, and manuscripts accessible to the public and will preserve these to the best of their ability, in perpetuity.

Please sign the following statement:

I hereby grant permission to the Graduate Division of the University of California, San Francisco to release copies of my thesis, dissertation, or manuscript to the Campus Library to provide access and preservation, in whole or in part, in perpetuity.

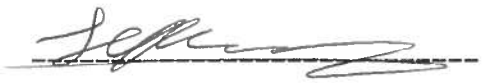

09/09/15

Author Signature Date